Proceeding Paper

Detection and Velocimetry of Floating Wood for Flood Disaster Risk Management Using Electromagnetic Imaging [†]

Christopher Gomez [1,2,]*[ ], Norifumi Hotta [3], Shusuke Miyata [4], Balazs Bradak [1][ ], Mikito Kataoka [1], Kensuke Ashikaga [1] and Frans C. Persendt [5]

[1] Sabo Laboratory, Faculty of Oceanology, Kobe University, Kobe City 658-0022, Japan; bradak.b@port.kobe-u.ac.jp (B.B.); kataokamikito@gmail.com (M.K.); footkenpenta179@gmail.com (K.A.)
[2] Centre of Natural Hazards and Disaster Risk, Gadjah Mada University, Yogyakarta 55281, Indonesia
[3] Department of Forest Science, Graduate School of Agricultural and Life Sciences, University of Tokyo, Tokyo 113-8654, Japan; hotta.norifumi@fr.a.u-tokyo.ac.jp
[4] Disaster Prevention Research Institute, Kyoto University, Kobe City 657-8501, Japan; miyata.shusuke.2e@kyoto-u.ac.jp
[5] Centre for Innovation in Learning and Teaching, University of Namibia, 340 Mandume Ndemufayo Avenue, Pionierspark, Windhoek 13301, Namibia; fpersendt@unam.na
* Correspondence: christophergomez@bear.kobe-u.ac.jp or kaikikazanbear@gmail.com
[†] Presented at the 4th International Electronic Conference on Geosciences, 1–15 December 2022; Available online: https://sciforum.net/event/IECG2022.

Abstract: Wood travelling in rivers is a major hazard to lives and infrastructures, because tons of wood material can travel nearing the speed of the flood flow. If post-event mapping, detection and numerical simulation have made important progress, detecting in-flow driftwood in all weather and at all times still presents several challenges. The present work aims to expand the capacity to detect in-flow wood by adapting the ground-penetrating radar electromagnetic method. The laboratory test was carried out over a water circulation flume using an 800 MHz nominal frequency antenna sampling at 100 Hz and a video camera set on top of the flume to measure the average velocity of the wood logs. A set of single wood logs of 20 cm in length travelled underneath the antenna. The GPR results have demonstrated that the method had the potential to detect moving wood, and that it could "see" underneath the water to the shallow flume floor. The experiments resulted in the ability to count wood travelling underneath the antenna, and the instantaneous velocity was obtained with velocities ranging from 0.307 to 0.352 m/s, which was slightly higher than the average velocity measured from video imaging. This difference is explained by the in-flow acceleration of the wood after its introduction into the flume.

Keywords: wood; driftwood; in-flow wood monitoring; radar; river; flood

1. Introduction

Wood located in channels and within the riverbed (Figure 1) has been demonstrated to play an essential geomorphic role in natural habitats [1], often putting ecological and economic goals in competition. Indeed, during historical periods, industrialized countries systematically cleared logjams from large waterways, as they can increase flooding and disrupt economic activities relying on waterways [2]. From a scientific and management perspective, wood also provides a proxy for the recruitment process in a river catchment, notably through the depositional patterns in the floodplain (i.e., single large or small pieces, single or racked jams, etc.) [3]. The size and the location of the wood in the stream, in turn, exerts control over the alternation between deposition and transport, with the mountain streams preferentially transporting wood during floods [4–6], while larger streams and rivers can also carry wood at mode flow [5]. The characterization and volume estimation of the wood in the floodplain and in the waterways mostly occurs in the aftermath of wood

travel and transport. It is achieved for wood trapped in water reservoirs behind dams using data from the volume removed by the hydro-electric companies [7], using historical and time-lapse cameras [7], using geometric calculations from field photographs of the deposits [8], and using digitization from post-flood deposits [9]. Even field research on the flowage of wood is dominated by work on deposited material [10], and the entrainment [11] and movement data are often obtained from laboratory and computer simulations [12–14].
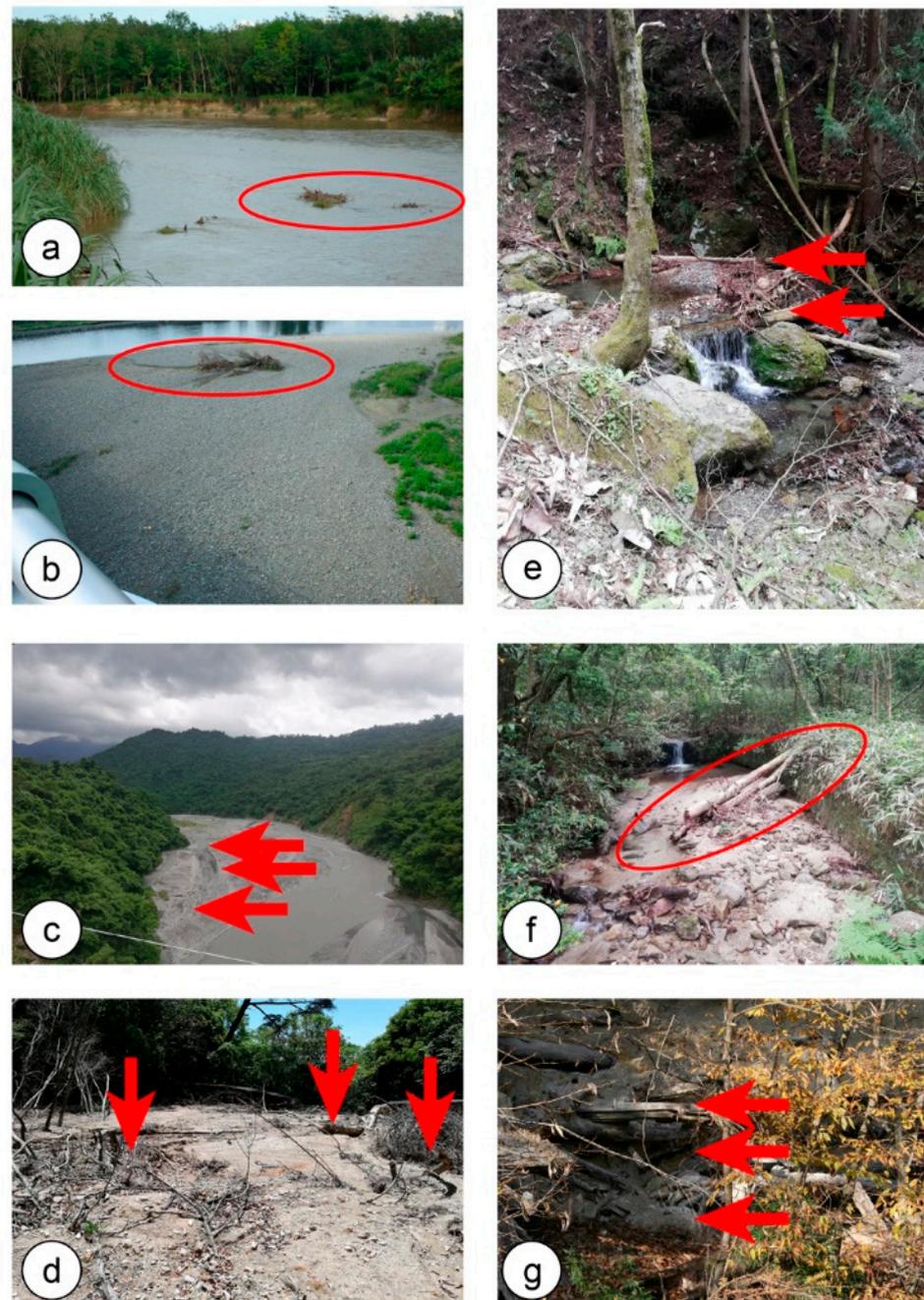
Figure 1. Wood in rivers of East Asia: (**a**) grounded debris in the Barumun River (Sumatra, Indonesia); (**b**) wood trapped in artificially reworked point bars in the Tamagawa River (Tokyo, Japan); (**c**) wood logs deposited in the swale of a point bar in South-Taiwan (China); (**d**) wood logs trapped inside a sediment check dam (sabo dam) in the Sumiyoshigawa River, Kobe, Japan; (**e**) wood in a mountain stream in the Gifu Prefecture (Japan); (**f**) a mountain stream in the Aichi Prefecture (Japan); and wood deposited by a pyroclastic flow and exhumed as a terrace in Numazawa (Japan); (**g**) trapped wood in a mountain stream of the Centerbury Region (New Zealand).

In the field, the in-flow log displacement has been resolved using RFID and GPS tracking devices implanted in or chained to the logs [14], notably allowing the authors to link the driftwood incipient motion to a 40% bankfull discharge.

However, wood monitoring using video cameras and photographs has been shown to be challenging in poor visibility conditions (even if positive results have been obtained at night under the right lighting conditions [15]), and most of this work relies on post-event imaging [16]. Another issue, which is still unresolved, is logjams and logs travelling underneath the water surface. To bridge this research gap, it is thus necessary to develop a monitoring method that can retrieve information at night, in the rain, and for material underneath the water. One instrument that is known to work at frequencies travelling in the air, the ground, and in freshwater is a ground-penetrating radar and, inversing the GPR variable to solve, the technique can be adapted to moving objects, as when a RADAR detects planes in the sky.

A ground-penetrating radar (GPR) is an electromagnetic method based on the propagation of electromagnetic waves in the ground. The antenna emits an electromagnetic signal, which is then propagated through the ground, mostly in relation to the dielectric permittivity of the material. The latter varies with a variety of factors (rock type, grain-size, amount of water, the presence of iron oxides, water, etc.), in such a way that the electromagnetic wave in a vacuum travelling at 0.3 m/ns travels at values usually beneath 1/3 of the velocity in a vacuum. The GPR is made of a signal generation and control system linked to an antenna with a nominal electromagnetic frequency ranging from 10 MHz to ~1000 MHz. The imaging of the studied medium is carried out by dragging the GPR antenna over the surface of a target, which then provides a representation of the internal structure of this medium. This image relies on the returned electric part of the electromagnetic signal. The ability of the radar to penetrate media beyond travelling in the air was randomly discovered by the US Air force when flying over Greenland and crashing into the ice, because the radar did not return the ice level, but the bedrock underneath. From this accident, researchers started to develop GPR to image ice thickness and characteristics [17], as well as ice and snow levels and density [18], before turning to soils and river environments: deposits architecture and related processes [19], floodplain structure [20], and faults through the floodplains [21], landslides' displacements [22], etc. GPR work also extended on the coastlines [23], as well as in more challenging environments in term of data acquisition and processing, such as in debris-flow deposits [24] and still-warm (600 degrees) pyroclastic flow deposits [25]. Outside of the field of geosciences, high-frequency antenna have also been instrumental when hitched to a truck to monitor highways' pavements [26], bridge structures, and tunnels [27], etc. All this research relies on a multitude of radar impulses stacked next to one another in order to image the internal architecture of an object, but there has also been research with the GPR antenna being kept immobile, in order to investigate the change in the radar signal, e.g., the relation between the GPR signal and snow wetness [28].

Nevertheless, there has not been any research on GPR as applied to moving water flows and moving objects in water. Instead of moving the antenna over a known distance, the space–time relation can be determined using the physics of electromagnetic waves. In the present contribution, we aim to prove that GPR technology can be used for the purpose of wood detection and velocimetry in a challenging environment, when it has not been possible to acquire direct data from other sensors or from sensors attached to the driftwood [13,14].

2. Experimental Setup and Methodology

In the present research, a Ground-Penetrating Radar Mala Reflex-ProX (Mala, Sweden), mounted with an antenna of a nominal frequency of 800 MHz, was set over a 0.2 m wide water circulation flume at 0.28 m above the water, which was 0.1425 m deep just underneath the antenna (Figure 2). The geometry of the water underneath during the flow had a cross-sectional area of 0.0285 m^2 and a wetted perimeter of 0.485 m for a slope of 0.00435 m/m.

The wood sections used in the present case were 0.2 m long and had a diameter of 0.008 m (Table 1). The average velocity of the driftwood was measured using the time between two points in the flume from video imagery. The video camera was located above the flume.
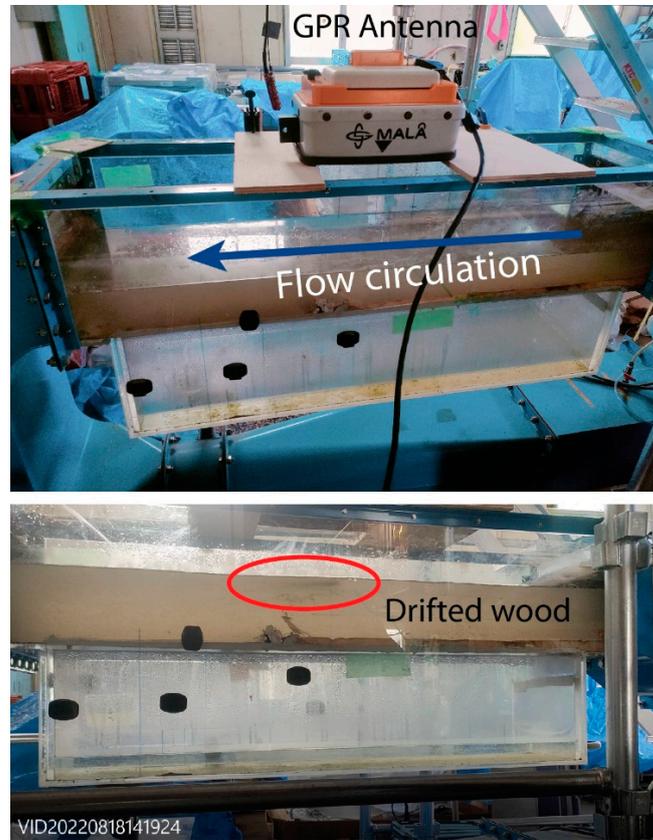
Figure 2. Instrumental setup in the laboratory with the driftwood being released and transported by the water underneath the 800 MHz antenna.

Table 1. Characteristics of the floated wood as well as the Manning water velocity estimates.

Floating Wood Characteristics					Manning Calculation of Velocity and Discharge					
Total Length	Wood φ	Wood L.	Wood Area	Velocity	Area	Wetted Perimeter	Slope	*n* (Artificial Laminated Chow, 1959)	Velocity	Discharge
[m]	[m]	[m]	[m^2]	[m/s]	[m^2]	[m]	[m/m]	[/]	[m/s]	[m^3/s]
1.15	0.008	0.2	0.01	0.25	0.0285	0.485	0.00435	0.02	0.50	0.01
1.15	0.008	0.2	0.01	0.2	0.0285	0.485	0.00435	0.02	0.50	0.01
1.15	0.008	0.2	0.01	0.25	0.0285	0.485	0.00435	0.02	0.50	0.01
1.15	0.008	0.2	0.01	0.25	0.0285	0.485	0.00435	0.02	0.50	0.01
1.15	0.008	0.2	0.01	0.25	0.0285	0.485	0.00435	0.02	0.50	0.01
1.15	0.008	0.2	0.01	0.2	0.0285	0.485	0.00435	0.02	0.50	0.01

The radargram was recorded in *rd3 and, from one single radargram, the six wood lengths that floated underneath the radar were confirmed with videos and soundtracks. The portion of the radargram was then exported to (1) remove the antenna-to-water surface region, so that the time 0 of each trace is at the water surface. (2) The DEWOW filter was applied to limit the effect of the surface penetration, and (3) horizontal repeats and noise were suppressed using a signal average removal, for which the average was calculated from every 100 traces (the choice was purely empirical, and based on the quality of different trial

and error). Moreover, (4) the signal amplitude was enhanced using the AGC gain. Finally, (5) using the known velocity of electromagnetic waves in fresh water (0.033 m/ns), the time of the returned signal was transformed into the depth of penetration (by also halving the two-way signal).

From the set of processing steps above, one has a set of hyperbolae created by the wood moving towards and away from the antenna. This is represented on the radargram by the traditional hyperbolae signals. Instead of attempting to calculate the velocity of the signal in the medium by relating the horizontal distance to the time it takes to reach a certain depth, the authors turned the method upside down and used the known velocity in the air/vacuum (not in the water, because the travel from the antenna to the wood is controlled by the travel in the air) to calculate the distance travelled for a known time-span in the air. These data were then converted into the velocity of each wood.

3. Results and Discussion

For the six wood samples, the observed wood velocity over a flume length of 1.1 m varied between 0.2 and 0.25 m/s, although these values are certainly underestimated as the wood was still being accelerated towards an equilibrium velocity. By comparison, the estimation made from the Manning's equation provided a water velocity of 0.49 m/s. (Table 2).

Table 2. Wood velocity calculation from the videos and numbering relating to the GPR hyperbolae.

Wood Velocity from Videos										
Nb	GPR	M Setup	Water Depth	Wood Velocity	In	Out	Distance	Time	Upstream Depth	Downstream Depth
[/]	[/]	[/]	[m]	[m/s]	[s]	[s]	[m]	[s]	[m]	[m]
1	8	75	0.1425	0.25	14	18	1	4	0.145	0.14
2	8	75	0.1425	0.2	19	24	1	5	0.145	0.14
3	8	75	0.1425	0.25	26	30	1	4	0.145	0.14
4	8	75	0.1425	0.25	31	35	1	4	0.145	0.14
5	8	75	0.1425	0.25	36	40	1	4	0.145	0.14
6	8	75	0.1425	0.2	41	44	0.6	3	0.145	0.14

Nb is the Number; M Setup is the Motor Setup; In and Out signify the time when the wood was introduced to and left the measurement area; Distance is the distance travelled by the wood for velocity calculation.

The 800 MHz GPR signal penetrated the water to the flume floor 0.1425 m underneath the water level (Figure 3). The depth was confirmed by plunging a ruler into the flume water. Due to the preparation time, the first piece of wood only passes underneath the antenna after 140 s, while the last one passes slightly after 170 s (Figure 3). The sixth piece of wood, although only 0.008 m in diameter, created a clear signal and as they did not flow in a straight line, but realigned themselves, this resulted in hyperbolae with several "heads" (further comparison is needed between the video and the GPR signal). For each hyperbola, the velocity calculation from the rising limb of the hyperbola (as the wood was still being accelerated this explains why the falling limb has a slightly different angle) provided velocities ranging from 0.307 to 0.380 m/s (Table 3), which is higher than the velocities recorded from the video data (0.2 to 0.25 m/ns of averaged velocity).
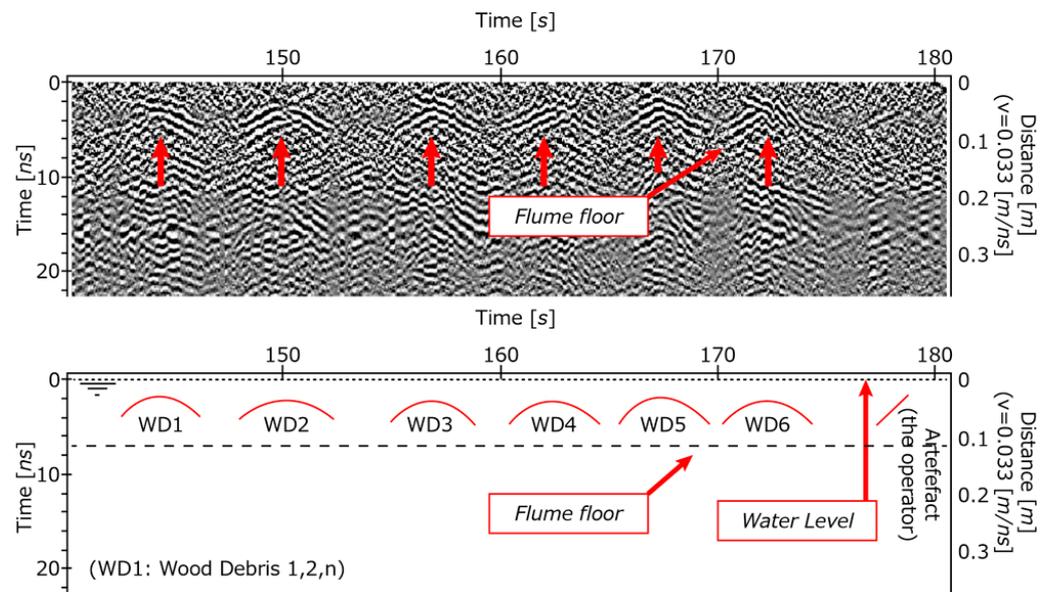
Figure 3. Original radargram after signal processing and explanation of the data has been extracted. The red arrows show the location of the driftwood when underneath the antenna.

Table 3. Calculation of velocities based on the hyperbolae slopes of the radargram.

Wood nb	Depth 1	Depth 2	x1	x2	Start	Timelapse	Triangulated Horizontal	Halved (Return to Single)	Nanosec. to Distance Using Light-Speed	Velocity
[/]	[ns]	[ns]	[1/100 s]	[1/100 s]	s	s	[ns]	ns	[m]	[m/s]
1.000	5.045	3.550	14,283	14,421	0.000	1.380	3.585	1.792	0.520	0.377
1.000	4.718	3.177	14,270	14,403	0.000	1.330	3.489	1.744	0.506	0.380
2.000	4.205	2.663	14,839	14,977	0.000	1.380	3.254	1.627	0.472	0.342
2.000	4.251	2.616	14,837	14,975	0.000	1.380	3.351	1.675	0.486	0.352
3.000	4.999	2.990	15,531	15,699	0.000	1.680	4.006	2.003	0.581	0.346
3.000	4.111	2.336	16,051	16,211	0.000	1.600	3.383	1.692	0.491	0.307

Depth 1 and 2 are the two vertical points from the hyperbolae used for calculation of the velocity; x1 and x2 are the horizontal elements of the same points. Timelapse is the time between x1 and x2.

4. Conclusions

The experiments show that: (1) wood can be counted via electromagnetic imaging; (2) the velocity of the wood can also be estimated, although the present experiments need to be run with a longer flume, so that the optimal velocity is attained; and (3) finally, the next step in the present research is to compare the falling and rising limb to calculate the acceleration of the wood.

Author Contributions: Conceptualization, methodology and analysis C.G.; formal analysis, C.G., N.H., S.M., M.K. and K.A.; writing—original draft preparation, C.G. and B.B.; writing—review and editing C.G., N.H., S.M. and F.C.P.; grant acquisition, N.H. All authors have read and agreed to the published version of the manuscript.

Institutional Review Board Statement: Not applicable.

Informed Consent Statement: Not applicable.

Data Availability Statement: Data are available upon request to the corresponding author, and should be made available once further experiments have been conducted.

Conflicts of Interest: The authors declare no conflict of interest.

References

1. Gunnell, A.M.; Petts, G.E.; Gregory, K.J. The role of coarse woody debris in forest aquatic habitats: Implications for management. *Aquat. Conserv.* **1995**, *5*, 143–166. [CrossRef]
2. Bisson, P.A.; Bilby, R.E.; Bryant, M.D.; Dollof, C.A.; Grette, G.B.; House, M.L.; Murphy, M.L.; Koski, K.V.; Sedell, J.R. Large woody debris in forested streams in the pacific northwest: Past, present and future. In *Streamside Management: Forestry and Fishery Interactions*; Saleo, E.O., Cunty, T.W., Eds.; University of Washington Publisher: Washington, DC, USA, 1987.
3. Abbe, T.M.; Montgommery, D.R. Patterns and processes of wood debris accumulation in the Queets river basin, Washington. *Geomorphology* **2003**, *51*, 81–107. [CrossRef]
4. Nakamura, F.; Swanson, F.J. Effects of coarse woody debris on morphology and sediment storage of a mountain stream system in western Oregon. *Earth Surf. Process. Landf.* **1993**, *18*, 46–61. [CrossRef]
5. Seo, J.; Nakamura, F.; Chun, K. Dynamics of large wood at the watershed scale: A perspective on current research limits and future directions. *Landsc. Ecol. Eng.* **2010**, *6*, 271–287. [CrossRef]
6. Chen, S.-C.; Chao, Y.-C.; Chan, H.-C. Typhoon-dominated influence on Wood Debris Distribution and Transportation in a High Gradient Headwater Catchment. *J. Mt. Sci.* **2013**, *10*, 509–521. [CrossRef]
7. Moulin, B.; Piegay, H. Characteristics and temporal variability of large woody debris trapped in a reservoir on the river Rhone (Rhone): Implications for river basin management. *Riv. Res. Appl.* **2004**, *20*, 79–97. [CrossRef]
8. Thevenet, A.; Citterio, A.; Piegay, H. A new methodology for the assessment of large woody debris accumulations on highly modified rivers (example of two French piedmont rivers). *Regul. Rivers Res. Mgmt.* **1998**, *14*, 467–483. [CrossRef]
9. Shimizu, M.; Kanai, S.; Hotta, N.; Lissak, C.; Gomez, C. Spatial Distribution of Drifted-wood Hazard following the July 2017 Sediment-hazards in the Akatani river, Fukuoka Prefecture, Japan. *For. Geo* **2020**, *34*, 96–111. [CrossRef]
10. Pettit, N.E.; Warfe, D.M.; Kennard, M.J.; Pusey, B.J.; Davies, P.M.; Douglas, M.M. Dynamics of in-stream wood and its importance as fish habitat in a large tropical floodplain river. *River Res. Appl.* **2013**, *29*, 864–875. [CrossRef]
11. Bocchiola, D.; Rulli, M.C.; Rosso, R. Flume experiments on wood entrainment in rivers. *Adv. Water Resour.* **2006**, *29*, 1182–1195. [CrossRef]
12. Panici, D. An Experimental and Numerical Approach to Modeling Large Wood Displacement in Rivers. *Water Resour. Res.* **2012**, *57*, e2021WR029860. [CrossRef]
13. Spreitzer, G.; Gibson, J.; Tang, M.; Tunnicliffe, J.; Friedrich, H. SmartWood: Laboratory experiments for assessing the effectiveness of smart sensors for monitoring large wood movement behaviour. *Catena* **2019**, *182*, 104145. [CrossRef]
14. Ravazzolo, D.; Mao, L.; Pico, L.; Lenzi, M.A. Tracking log displacement during floods in the Tagliamento River using RFID and GPS tracker devices. *Geomorph* **2015**, *228*, 226–233. [CrossRef]
15. Ghaffarian, H.; Piegay, H.; Lopez, D.; Riviere, N.; MacVicar, B.; Antonio, A.; Mignot, E. Video-monitoring of wood discharge: First inter-basin comparisonand recommendations to install video cameras. *Earth Surf. Process Landforms* **2020**, *45*, 2219–2234. [CrossRef]
16. MacVicar, B.; Piegay, H. Implementation and validation of video monitoring for wood budgeting in a wandering piedmont river, the Ain River (France). *Earth Surf. Process Landforms* **2012**, *37*, 1272–1289. [CrossRef]
17. Galley, R.J.; Trachtenberg, M.; Langlois, A.; Barber, D.G.; Shafai, L. Observations of geophysical and dielectric properties and ground penetrating radar signatures for discrimination of snow, sea ice and freshwater ice thickness. *Cold Reg. Sci. Technol.* **2009**, *57*, 29–38. [CrossRef]
18. Jaedicke, C. Snow mass quantification and avalanche victim search by ground penetrating radar. *Surv. Geophys.* **2003**, *24*, 431–445. [CrossRef]
19. Huber, E.; Birte, A.; Huggenberger, P. Imaging scours in straightened and braided gravel-bed rivers with ground-penetrating radar. *Near Surf. Geophys.* **2019**, *17*, 263–276. [CrossRef]
20. Bakker, M.A.J.; Maljers, D.; Weerts, H.J.T. Ground-penetrating radar profiling on embanked floodplains. *Neth J. Geosci.* **2007**, *86*, 55–61. [CrossRef]
21. Wyatt, D.E.; Temples, T.J. Ground-penetrating radar detection of small-scale channels, joints and faults in the unconsolidated sediments of the Atlantic Coastal Plain. *Environ. Geol.* **1999**, *27*, 219–225. [CrossRef]
22. Lissak, C.; Maquaire, O.; Malet, J.-P.; Lavigne, F.; Virmoux, C.; Gomez, C.; Davidson, R. Ground-penetrating radar observations for estimating the vertical displacement of rotational landslides. *Nat. Hazards Earth Syst. Sci.* **2015**, *15*, 1399–1406. [CrossRef]
23. Kain, C.; Gomez, C.; Wassmer, P.; Lavigne, F.; Hart, D. Truncated dunes as evidence of the 2004 tsunami in North Sumatra and environmental recovery post-tsunami. *N. Z. Geogr.* **2014**, *70*, 165–178. [CrossRef]
24. Starheim, C.A.; Gomez, C.; Harrison, J.; Kain, C.; Brewer, N.J.; Owen, K.; Hadmoko, D.S.; Purdie, H.; Zawar-Reza, P.; Owens, I.; et al. Complex internal architecture of a debris-flow deposit revealed using ground-penetrating radar, Cass, New Zealand. *N. Z. Geogr.* **2013**, *69*, 26–38. [CrossRef]

25. Gomez, C.; Lavigne, F.; Lespinasse, N.; Hadmoko, D.S.; Wassmer, P. Longitudinal structure of pyroclastic-flow deposits, revealed by GPR survey, at Merapi Volcano, Java, Indonesia. *J. Volcanol. Geotherm. Res.* **2008**, *176*, 439–447. [CrossRef]
26. Guo, S.; Xu, Z.; Li, X.; Zhu, P. Detection and Characterization of Cracks in Highway Pavement with the Amplitude Variation of GPR Diffracted Waves: Insights from Forward Modeling and Field Data. *Remote Sens.* **2022**, *14*, 976. [CrossRef]
27. Hugenschmidt, J. Concrete bridge inspection with a mobile GPR system. *Constr. Build. Mat.* **2002**, *16*, 147–154. [CrossRef]
28. Granlund, N.; Lundberg, A.; Feiccabrino, J.; Gustafsson, D. Laboratory test of snow wetness influence on electrical conductivity measured with ground penetrating radar. *Hydrol. Res.* **2009**, *40*, 33–44. [CrossRef]